CHEMISTRY
A EUROPEAN JOURNAL

DOI: 10.1002/chem.201001789

Structural Effects of Fe_3O_4 Nanocrystals on Peroxidase-Like Activity

Shanhu Liu, Feng Lu, Ruimin Xing, and Jun-Jie Zhu*[a]

Abstract: The catalytic activity of nanocrystal catalysts depends strongly on their structures. Herein, we report three distinct structures of Fe_3O_4 nanocrystals, cluster spheres, octahedra, and triangular plates, prepared by a similar hydrothermal procedure. Additionally, the three Fe_3O_4 nanostructures were used as peroxidase nanomimetics and the correlation between the catalytic activities and the structures was first explored by using 3,3′,5,5′-tetramethylbenzidine and H_2O_2 as peroxidase substrates. The results showed that the peroxidase-like activities of the Fe_3O_4 nanocrystals were structure dependent and followed the order cluster spheres > triangular plates > octahedra; this order was closely related to their preferential exposure of catalytically active iron atoms or crystal planes. Such investigation is of great significance for peroxidase nanomimetics with enhanced activity and utilization.

Keywords: enzyme catalysis · magnetite · nanomaterials · peroxidase nanomimetics · structural effects

Introduction

Natural enzymes are the proteins that catalyze chemical reactions and they are incredibly efficient and highly specific biocatalysts under mild conditions. However, practical applications are largely limited because of their lack of stability and loss of activation in harsh chemical environment (e.g., nonphysiological pH, high temperature, and in the presence of inhibitors).[1–4] Therefore, artificial enzymes have attracted intensive attention due to their stability and effective enzyme-like catalysis over a wide range of temperatures and pH values compared with natural enzymes. Since magnetite nanoparticles were serendipitously discovered to have intrinsic peroxidase-like activity, they have been persued as peroxidase nanomimetics to catalyze and detect some molecules.[5–7] In addition, several kinds of the nanomaterials with enzyme-like activity have been reported.[8–11] However, there have been few attempts to investigate the catalytic properties of peroxidase nanomimetics with different structures and little is known about the effects of different nanostructures on biocatalysis with Fe_3O_4.

The intrinsic properties of nanocrystals are mainly determined by their composition, crystallinity, and structure. It is of great importance to investigate the structure-sensitive catalytic activity for obtaining a profound understanding of catalytic processes.[12–16] Much success has been achieved in the investigation of the structural effects of nanocrystals on catalysis and the results showed that the catalytic performance could be specifically regulated either by the crystal size or morphology with distinct crystallographic planes.[17–21] The reason might be that different crystal sizes or planes exhibit different numbers of dangling bonds and different atom arrangement manners, which intrinsically determine the reactivity and selectivity of catalysts. For instance, Co_3O_4 nanosheets with exposed {112} planes exhibited enhanced catalytic activity for methane combustion than Co_3O_4 nanobelts with {011} planes and nanocubes with {001} planes.[22] Also, CuCl crystallites with a preponderance of {111} crystal planes have better catalytic activity in aniline coupling than those with more {110} planes.[23] However, nanocrystal catalysts with different exposed crystal planes are usually decorated by a variety of capping agents, which undermines, to varying degrees, their catalytic activities for targets.[24,25] Therefore, different nanostructures with distinct crystallographic planes, provided that they could be prepared under the same or similar reaction systems, would be desired as model catalysts for comparison purposes.

Herein, we described the structure-controlled synthesis of Fe_3O_4 nanocrystals under a similar hydrothermal procedure.

[a] S. Liu, F. Lu, Dr. R. Xing, Prof. J.-J. Zhu
Key Laboratory of Analytical Chemistry for Life Science
Ministry of Education of China
School of Chemistry and Chemical Engineering
Nanjing University, Nanjing 210093 (P.R. China)
Fax: (+86) 2-583-594-976
E-mail: jjzhu@nju.edu.cn

Supporting information for this article is available on the WWW under http://dx.doi.org/10.1002/chem.201001789.

This imparts a significant advantage over Fe_3O_4 nanocrystals previously prepared in different ways. Furthermore, the obtained nanostructures were used as peroxidase nanomimetics towards typical substrates, such as 3,3′,5,5′-tetramethylbenzidine (TMB) and *o*-phenylenediamine (OPD), in the presence of H_2O_2. The structural effects on their peroxidase-like activities were investigated, which is highly significant for their application with enhanced activity and utilization.

Results and Discussion

Characterization of Fe_3O_4 nanocrystals with distinct structures: The crystal structures and crystallinity of three Fe_3O_4 nanostructures were determined by X-ray powder diffraction (XRD). As shown in Figure 1, all of the obtained products exhibited high crystalline quality; they were indexed to the face-centered-cubic (fcc) magnetite, in good agreement with the reported data (JCPDS no. 01-1111) and no impurity peaks were observed. More specifically, the product of the cluster spheres exhibited broader diffraction peaks, and the crystal size was about 15 nm by calculation with the Debye–Scherrer formula for its {311} peak.[10]

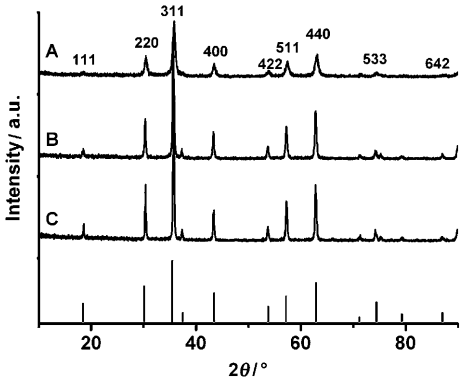

Figure 1. XRD patterns of the obtained Fe_3O_4 nanocrystals with different structures: cluster spheres (A), triangular plates (B), and octahedra (C).

The morphology, dimensions, and structural characteristics of the products were found to depend strongly on the amount of CH_3ONa and water in the reaction system, characterized by SEM and TEM. When the amount of CH_3ONa was 40 mmol, the product was dominated by cluster spheres with secondary structure as shown in Figure 2A; a statistical analysis yielded an average size of 170 nm in diameter. The cluster spheres were composed of many primary magnetite crystallites approximately 13 nm in size, consistent with the XRD anaylsis. The TEM image in Figure 2B further confirmed the secondary structure of the cluster spheres. Figure 2C showed that the lattice fringes were 0.253 nm, in good agreement with the values for {311} planes of cubic magnetite phase; and the same crystal orientation of different magnetite crystallites was observed.[26] The selected-area electron diffraction (SAED) pattern recorded on a single cluster sphere revealed its crystalline nature (Figure S1A in the Supporting Information). With increasing the amount of CH_3ONa to 50 mmol, the product developed the morphology of octahedra and the edge lengths were in the range of 120–140 nm as shown in Figure 2D. The octahedra exhibited a well-defined shape with smooth surfaces (Figure 2E). The distances between two adjacent planes were 0.495 nm, analogous to the (111) planes of cubic magnetite (Figure 2F). The corresponding SAED pattern revealed the single-crystalline nature of the octahedron (Figure S1B in the Supporting Information). Therefore, it could be concluded that each octahedron was a single crystal enclosed by eight {111} planes.[27,28] In addition, triangular plates were obtained by further adding water (1 mL) to the initial reaction solution of the octahedra system. Both SEM and TEM images showed that triangular plates were obtained as the major product (75%), with edge lengths of approximately 140 nm as shown in Figure 2G and H. The typical lattice fringe spacings of triangular plates were determined to be 0.299 nm, corresponding to the {220} *d* spacing of cubic magnetite (Figure 2I), consistent with its SAED anaylsis (Figure S1C in the Supporting Information). Although the mechanism for the structural evolution is still under investigation, alkalinity-related kinetic considerations might be responsible for the preferential absorption of some molecules (such as formate) on different crystal facets. This might direct the growth of nanoparticles into various structures by controlling the growth rates along various crystallographic directions.[29,30]

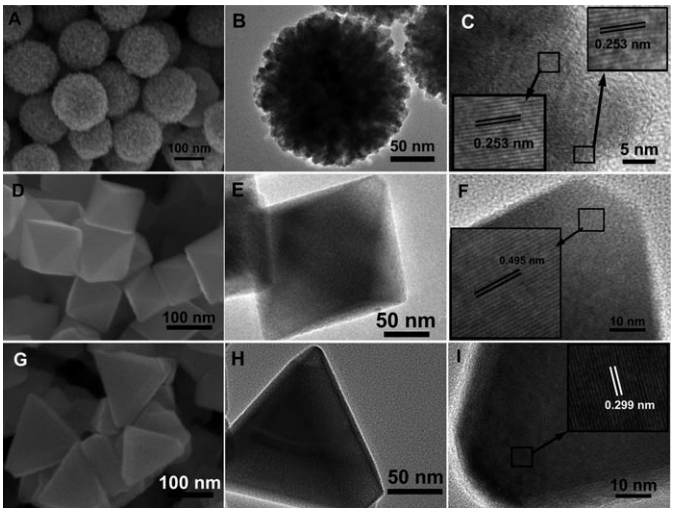

Figure 2. Typical SEM (A, D, G), TEM (B, E, H) and high-resolution TEM (C, F, I) images of the obtained Fe_3O_4 nanocrystals with different structures. A–C) Cluster spheres, E–F) octahedra, and G–I) triangular plates.

The magnetic properties of the three Fe_3O_4 nanostructures were studied by using a commercial superconducting quantum interference device (SQUID) magnetometer at room temperature. Figure 3 shows the hysteresis loops of these nanostructures at 300 K obtained by cycling the field between −10 and 10 kOe. All of them exhibited significant

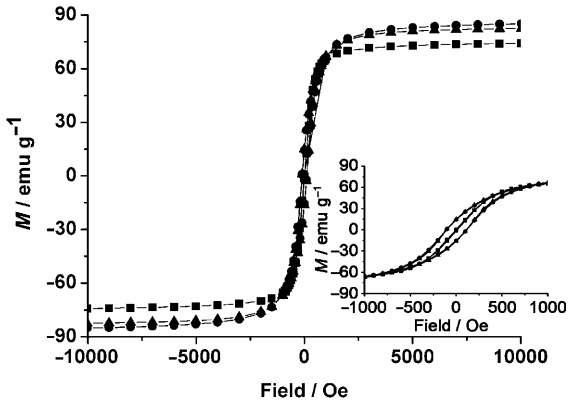

Figure 3. Room-temperature magnetization curves as a function of field for cluster sphere (■), triangular plate (●), and octahedral (▲) Fe_3O_4 nanostructures.

magnetization and the saturation magnetization values were 75.9, 87.4, and 83.5 emu g^{-1} for cluster spheres, triangular plates, and octahedra, respectively. Furthermore, it is worth mentioning that the cluster spheres exhibited superparamagnetic properties and no clear remanence or coercivity was found, as shown in the inset of Figure 3. It is believed that the threshold size for Fe-based nanoparticles is about 25 nm for the transition from superparamagnetism to ferromagnetism.[31,32] Therefore, the magnetic properties further confirmed that the cluster spheres were made up of primary magnetite crystallites. Whereas the other two nanostructures revealed a typical ferromagnetic behavior; a remanence of 15 emu g^{-1} and a coercivity of 100 Oe were observed from their hysteresis loops.

The oxidation of peroxidase substrates catalysed by the Fe_3O_4 nanocrystals: The natural peroxidases typically catalyze the oxidation of a substrate to develop a color change in the presence of H_2O_2. First, TMB and H_2O_2 were used to test the catalytic activity of the Fe_3O_4 nanocrystals with distinct structures. As shown in Figure 4, in the absence of

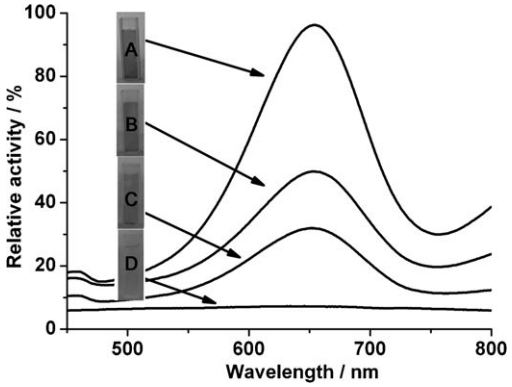

Figure 4. Typical photographs and relative activity of TMB-derived oxidation product, in the presence of H_2O_2, catalysed by the Fe_3O_4 nanocrystals with different structures or without Fe_3O_4: A) cluster spheres, B) triangular plates, C) octahedra, and D) without Fe_3O_4.

Fe_3O_4, a colorless solution containing TMB and H_2O_2 was observed and presented a negligible absorption in the range from 450 to 800 nm. In contrast, in the presence of any of Fe_3O_4 nanostructures, the solutions developed a blue color and exhibited similar spectral features with their characteristic absorbance at 652 nm, except for the variations in absorbance intensity. This absorption arises from the oxidation product of TMB, similar to the phenomena observed for the commonly used horse radish peroxidase enzyme.[1] The intensity might have relevance to the catalytic activities of different Fe_3O_4 nanostructures. In addition, similar catalytic performance was observed when OPD was used as the substrate in place of TMB. As shown in Figure 5, without Fe_3O_4

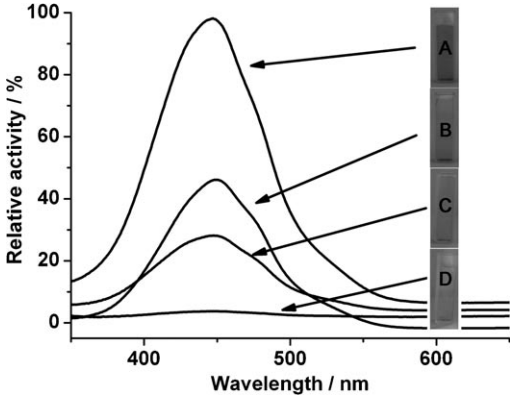

Figure 5. Typical photographs and relative activity of OPD-derived oxidation product, in the presence of H_2O_2, catalysed by the Fe_3O_4 nanocrystals with different structures or without Fe_3O_4: A) cluster spheres, B) triangular plates, C) octahedra, and D) without Fe_3O_4.

nanocrystals, there was still a colorless solution containing OPD and H_2O_2 with an insignificant absorbance in the measured range. In contrast, with any of Fe_3O_4 nanocrystals, the solutions gave an orange color with maximum absorbance at 450 nm, which originated from the oxidation product of OPD;[1] but there was still a difference in absorbance intensity for different Fe_3O_4 nanostructures. These results indicated that the Fe_3O_4 nanocrystals had peroxidase-like activity towards typical peroxidase substrates, such as TMB and OPD, in the presence of H_2O_2; but different Fe_3O_4 nanostructures might exhibit different catalytic activities. The possible reaction mechanism was speculated to be that shown in Scheme 1.

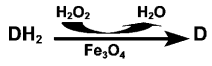

Scheme 1. The possible reaction mechanism of the oxidation of peroxidase substrates in the presence of H_2O_2, catalysed by the Fe_3O_4 nanocrystals. DH_2 is a substrate that is a hydrogen donor.

pH-, temperature-, and structure-dependent catalytic activities of the Fe_3O_4 nanocrystals: To investigate the catalytic activities of different Fe_3O_4 nanostructures, the substrates TMB and H_2O_2 were selected for use in a model system in the following experiments. To acquire an optimal response,

the effects of pH and temperature on the catalytic activities of the Fe_3O_4 nanocrystals were investigated. The pH varied from 2 to 10 and the temperature from 25 to 80 °C. The response curves in Figure 6 show that the optimized catalytic

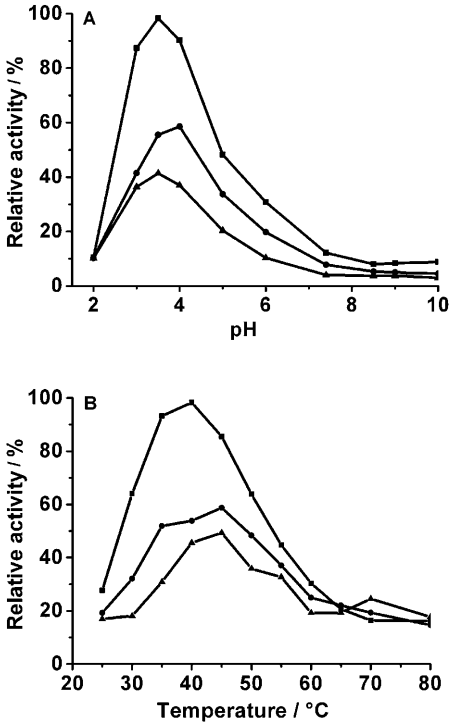

Figure 6. Effects of pH (A) and temperature (B) on the catalytic response of the cluster sphere (■), triangular plate (●), and octahedral (▲) Fe_3O_4 nanocrystals with the substrates TMB and H_2O_2.

conditions are approximately pH 4.0 and 40 °C. To exclude the possibility of leaching of iron ions from the Fe_3O_4 nanocrystals into the reaction solution, the Fe_3O_4 nanocrystals were incubated in standard reaction buffer (pH 4.0) and then removed by an external magnet. The absorption curves of the leaching solutions were tested. All of the leaching solutions presented a negligible absorption, indicating that the observed peroxidase-like activities were derived from the Fe_3O_4 nanocrystals themselves rather than as a result of iron leaching.

Figure 7 shows the time-dependent catalytic activity of different Fe_3O_4 nanostructures under the optimized catalytic conditions (pH 4.0 and 40 °C). The different Fe_3O_4 nanostructures showed different levels of activity over the reaction time, in the order of cluster spheres > triangular plates > octahedra, and the plateaus appeared within 30 min. The Michaelis constants (K_m) were determined to explore the correlation between the structures and the activities. As summarized in Table 1, the K_m value of the cluster spheres with TMB as the substrate was about two times lower than that of the triangular plates and 2.5 times lower than that of the octahedra. The results indicated that the cluster spheres had the highest affinity for TMB and the triangular plates

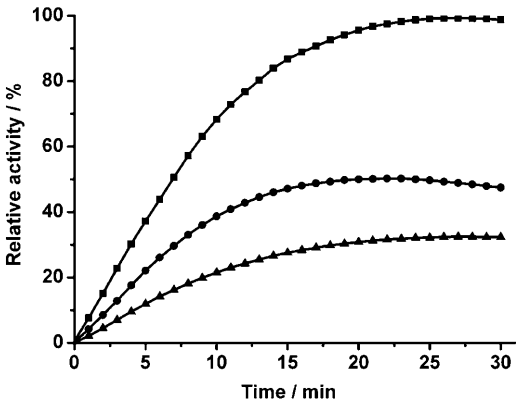

Figure 7. A time-dependent catalytic activity of cluster sphere (■), triangular plate (●), and octahedral (▲) Fe_3O_4 nanostructures with TMB and H_2O_2 as the substrates under the optimized conditions (i.e., 0.2 M acetate buffer, pH 4.0 at 40 °C).

Table 1. Comparison of the structural characteristics and the K_m values of different Fe_3O_4 nanostructures.

Nanostructures	Specific surface area [$m^2 g^{-1}$][a]	Exposed planes	K_m [mM]
cluster spheres	34.5	{311}	0.23
triangular plates	11.7	{220}	0.46
octahedra	9.1	{111}	0.58

[a] Based on BET surface area analysis.

exhibited medium affinity, higher than the octahedra. According to the structural analysis mentioned above, although the sizes of the three Fe_3O_4 nanostructures were similar in dimension, the cluster spheres were composed of many primary particles and displayed larger specific surface areas than the triangular plates and the octahedra according to BET analysis (in Table 1). For the cluster spheres, more catalytically active iron atoms at the surface interacted with the substrate; therefore, the cluster spheres exhibited the highest activity. In addition, although the size and surface area of the triangular plates were close to those of the octahedra, the surface atom arrangements of {220} and {111} planes were quite different, as shown in Figure S2 in the Supporting Information. The atomic structure of the former might be a more reactive surface due to its more open plane and dangling bonds;[22,30,33,34] accordingly, the triangular plates with {220} planes exhibited a superior catalytic activity to the octahedra with {111} planes.

Reusability of the Fe_3O_4 nanocrystals as peroxidase nanomimetics: The Fe_3O_4 nanocrystals, as a kind of inorganic materials, are expected to be more thermally and chemically stable than natural peroxidases. To investigate their reusability as peroxidase nanomimetics, the recycling catalysis experiments of the cluster spheres were carried out and the catalytic activity was examined in each cycle. As shown in Figure 8, only a small decrease in the absorbance was observed after seven successive cycles, with no significant reduction as a whole. SEM micrographs of the cluster spheres

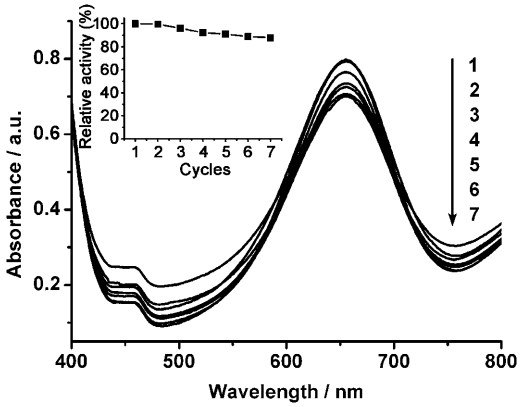

Figure 8. The catalytic activity of the cluster spheres in seven successive recycling catalysis. The inset shows the conversion of the catalytic activity with the first run as 100%.

after recycling catalysis in Figure S3 in the Supporting Information showed that the morphology and dimension of the cluster spheres remained unchanged, and no clear agglomeration was observed. The small decrease in the absorbance was presumed to be as a result of gradual loss of the cluster spheres due to repeated magnetic separations. This indicates that the cluster spheres were stable and exhibited excellent reusability in the catalysis process; they might be superior to individual aggregation-prone primary particles in terms of stability and recycling utilization.

Conclusion

Fe_3O_4 nanocrystals with different structures, cluster spheres, octahedra, and triangular plates, have been successfully fabricated by a similar hydrothermal procedure. These different Fe_3O_4 nanostructures had different specific surface areas and exposed crystal planes, and thus exhibited different levels of peroxidase-like activities, in the order of cluster spheres > triangular plates > octahedra; this order was closely related to their preferential exposure of catalytically active iron atoms or crystal planes. This indicates that selective fabrication of peroxidase nanomimetics with different structures is very important to harness their catalytic activities. This investigation is of particular significance for mechanistic understanding and technological applications of peroxidase nanomimetics for biotechnology, environmental chemistry, and medicine.

Experimental Section

Materials and preparation: TMB and OPD were purchased from Sigma–Aldrich. Hydrogen peroxide (30%) was from Shanghai Biochemical Reagent $FeCl_3{\cdot}6H_2O$, anhydrous NaAc, ethylene glycol (EG), and other chemical reagents were of analytical grade and used as received without further purification. All solutions were prepared with deoxygenated doubly distilled water.

Typical synthesis of the Fe_3O_4 nanocrystals with different structures: Fe_3O_4 cluster spheres were fabricated by hydrothermal treatment as follows: $FeCl_3$ (5 mmol) was dissolved in EG (40 mL) to form a clear solution, followed by the addition of anhydrous CH_3ONa (40 mmol). The mixture was vigorously mixed by ultrasonication to give a homogeneous solution. Then the solution was transferred to a Teflon-lined stainless steel autoclave (50 mL capacity) for hydrothermal treatment at 200°C for 10 h. After the autoclave was allowed to cool to room temperature, the precipitates were collected by magnetic separation and washed several times with water and ethanol under sonication, then dried under vacuum at room temperature before characterization and application. In addition, the reactants were adjusted to 50 mmol of CH_3ONa, and 50 mmol of CH_3ONa associated with 1 mL of water, and the rest of the synthesis conditions were kept the same as those mentioned above for the fabrication of octahedra and triangular plates, respectively.

Characterization: Field-emission SEM images were obtained by using a Hitachi S-4800 field-emission electron microscope at an accelerating voltage of 5 kV. TEM images and the corresponding SAED patterns were taken by using a JEOL JEM-2100 transmission electron microscope at an accelerating voltage of 200 kV. XRD measurements were performed on a Japan Shimadzu XRD-6000 diffractometer with $Cu_{K\alpha}$ radiation ($\lambda =$ 0.15418 nm); a scanning rate of $0.05°\,s^{-1}$ was applied to record the patterns in the 2θ range of 10–70°.

Peroxidase-like catalytic experiments of the Fe_3O_4 nanocrystals with different structures: The peroxidase-like activities of the Fe_3O_4 nanocrystals with different structures were examined in acetate buffer (2 mL; 0.2 M, pH 4.0) containing Fe_3O_4 nanocrystals (50 μM), in the presence of H_2O_2 (530 mM) and TMB (816 μM). The reactions were monitored in wavelength-scan mode or time-scan mode at 652 nm by using a Shimadzu UV-3600 spectrometer. Assays were carried out under the optimized conditions as described above by varying the concentrations of TMB and maintaining a fixed concentration of H_2O_2. The apparent steady-state reaction rates of three Fe_3O_4 nanostructures were deduced according to their absorbance data and the molar absorption coefficient of $39000\,M^{-1}cm^{-1}$ for TMB-derived oxidation products[34]. The reaction rates were fitted to the Michaelis equation to extract the Michaelis constants (K_m). The reusability of the Fe_3O_4 nanocrystals as peroxidase nanomimetics were investigated by using cluster spheres as an example. The catalytic activity was examined in each cycle after incubation and magnetic separation of the used cluster spheres. The separated cluster spheres were rinsed with deionized water and used in the next cycle; seven cycles were conducted in all.

Acknowledgements

This study was supported by the National Natural Science Foundation of China (20635020, 20821063) and National Basic Research Program of China (2006CB933201, 2011CB933502).

[1] L. Z. Gao, J. Zhuang, L. Nie, J. B. Zhang, Y. Zhang, N. Gu, T. H. Wang, J. Feng, D. L Yang, S. Perrett, X. Y. Yan, *Nat. Nanotechnol.* **2007**, *2*, 577–583.
[2] J. M. Perez, *Nat. Nanotechnol.* **2007**, *2*, 535–536.
[3] M. J. Banholzer, J. E. Millstone, L. Qin, C. A. Mirkin, *Chem. Soc. Rev.* **2008**, *37*, 885–897.
[4] L. Zhang, Q. Zhang, J. H. Li, *Adv. Funct. Mater.* **2007**, *17*, 1958–1965.
[5] H. Wei, E. K. Wang, *Anal. Chem.* **2008**, *80*, 2250–2254.
[6] S. Nath, C. Kaittanis, V. Ramachandran, N. S. Dalal, J. M. Perez, *Chem. Mater.* **2009**, *21*, 1761–1767.
[7] F. Q. Yu, Y. Z. Huang, A. J. Cole, V. C. Yang, *Biomaterials* **2009**, *30*, 4716–4722.
[8] Y. J. Song, X. H. Wang, C. Zhao, K. G. Qu, J. S. Ren, X. G. Qu, *Chem. Eur. J.* **2010**, *16*, 3617–3621.
[9] Z. Y. Chen, L. Xu, Y. Liang, M. P. Zhao, *Adv. Mater.* **2009**, *22*, 1488–1492.

[10] A. Asati, S. Santra, C. Kaittanis, S. Nath, J. M. Perez, *Angew. Chem.* **2009**, *121*, 2344–2348; *Angew. Chem. Int. Ed.* **2009**, *48*, 2308–2312.
[11] H. M. Fan, J. B. Yi, Y. Yang, K. W. Kho, H. R. Tan, Z. X. Shen, J. Ding, X. W. Sun, M. C. Olivo, Y. P. Feng, *ACS Nano* **2009**, *3*, 2798–2808.
[12] Y. G. Sun, Y. N. Xia, *Science* **2002**, *298*, 2176–2179.
[13] N. Tian, Z. Y. Zhou, S. G. Sun, Y. Ding, Z. L. Wang, *Science* **2007**, *316*, 732–735.
[14] Y. Zeng, R. Hao, B. Xing, Y. L. Hou, Z. Xu, *Chem. Commun.* **2010**, *46*, 3920–3922.
[15] X. W. Xie, Y. Li, Z. Q. Liu, M. Haruta, W. J. Shen, *Nature* **2009**, *458*, 746–749.
[16] D. Kim, N. Lee, M. Park, B. H. Kim, K. An, T. Hyeon, *J. Am. Chem. Soc.* **2008**, *130*, 454–455.
[17] Y. Lee, A. Loew, S. H. Sun, *Chem. Mater.* **2010**, *22*, 755–761.
[18] T. Xu, X. Zhou, Z. Y. Jiang, Q. Kuang, Z. X. Xie, L. S. Zheng, *Cryst. Growth Des.* **2008**, *8*, 192–196.
[19] X. G. Han, M. S. Jin, S. F. Xie, Q. Kuang, Z. Y. Jiang, Y. Q. Jiang, Z. X. Xie, L. S. Zheng, *Angew. Chem.* **2009**, *121*, 9344–9347; *Angew. Chem. Int. Ed.* **2009**, *48*, 9180–9183.
[20] H. G. Yang, G. Liu, S. Z. Qiao, C. H. Sun, Y. G. Jin, S. C. Smith, J. Zou, H. M. Cheng, G. Q. Lu, *J. Am. Chem. Soc.* **2009**, *131*, 4078–4083.
[21] D. B. Fan, P. J. Thomas, P. O'Brien, *J. Am. Chem. Soc.* **2008**, *130*, 10892–10894.
[22] L. H. Hu, Q. Peng, Y. D. Li, *J. Am. Chem. Soc.* **2008**, *130*, 16136–16137.
[23] T. Xie, M. Gong, Z. Niu, S. Li, X. Yan, Y. D. Li, *Nano Res.* **2010**, *3*, 174–179.
[24] R. Narayanan, M. A. El-Sayed, *J. Phys. Chem. B* **2005**, *109*, 12663–12676.
[25] H. Lee, S. E. Habas, S. Kweskin, D. Butcher, G. A. Somorjai, P. Yang, *Angew. Chem.* **2006**, *45*, 7824–7828; *Angew. Chem. Int. Ed.* **2006**, *45*, 7988–7992.
[26] S. H. Liu, R. M. Xing, F. Lu, R. K. Rana, J. J. Zhu, *J. Phys. Chem. C* **2009**, *113*, 21042–21047.
[27] B. Lim, M. Jiang, J. Tao, P. H. C. Camargo, Y. Zhu, Y. N. Xia, *Adv. Funct. Mater.* **2009**, *19*, 189–200.
[28] L. J. Zhao, H. J. Zhang, Y. Xing, S. Y. Song, S. Y. Yu, W. D. Shi, X. M. Guo, J. H. Yang, Y. Q. Lei, F. Cao, *Chem. Mater.* **2007**, *19*, 198–204.
[29] Z. L. Wang, *J. Phys. Chem. B* **2000**, *104*, 1153–1175.
[30] X. J. Zhang, C. Dong, J. Zapien, S. Ismathullakhan, Z. H. Kang, J. S. Jie, X. H. Zhang, J. Chang, C. S. Lee, S. T. Lee, *Angew. Chem.* **2009**, *121*, 9285–9287; *Angew. Chem. Int. Ed.* **2009**, *48*, 9121–9123.
[31] R. Hao, R. J. Xing, Z. C. Xu, Y. L. Hou, S. Gao, S. H. Sun, *Adv. Mater.* **2010**, *22*, 2729–2742.
[32] X. Hong, J. Li, M. J. Wang, J. J. Xu, W. Guo, J. H. Li, Y. B. Bai, T. J. Li, *Chem. Mater.* **2004**, *16*, 4022–4027.
[33] K. B. Zhou, X. Wang, X. M. Sun, Q. Peng, Y. D. Li, *J. Catal.* **2005**, *229*, 206–212.
[34] Y. Ding, F. R. Fan, Z. Q. Tian, Z. L. Wang, *Small* **2009**, *5*, 2812–2815.
[35] H. B. Dunford, *Biochemistry* **1997**, *36*, 9349–9355.

Received: June 24, 2010
Published online: November 29, 2010

